Combining MODIS and AMSR-E based vegetation moisture retrievals for improved fire risk monitoring

Swarvanu Dasgupta[a] and John J. Qu[a]

[a] Eastfire Lab, George Mason University, 4400 University Drive, Fairfax, Virginia, USA

ABSTRACT

Research has shown that remote sensing in both the optical and microwave domain has the capability of estimating vegetation water content (VWC). Though lower in spatial resolution than MODIS optical bands, AMSR-E microwave measurements are typically less affected by clouds, water vapor, aerosol or solar illumination, making them complementary to MODIS real time measurements over regions of clouds and haze. In this study we explored a wavelet based approach for combining vegetation water content observations derived from higher spatial resolution MODIS and lower spatial resolution AMSR-E microwave measurements. Regression analysis between AMSR-E VWC and spatially aggregated MODIS NDII (Normalized Difference Infrared Index) was first used to scale MODIS NDII to MODIS VWC products. Our approach for combining information from the two sensors resorts to multiresolution wavelet decomposition of MODIS VWC into a set of detail images and a single approximation image at AMSR-E resolution. The substitution method of image fusion is then undertaken, in which the approximation image is replaced by AMSR-E VWC image, prior to using inverse wavelet transform to construct a merged VWC product. The merged VWC product thus has information from both MODIS and AMSR-E measurements. The technique is applied over low vegetation regions in Texas grasslands to obtain merged VWC products at intermediate resolutions of ~1.5km. Apart from offering a way to calibrate MODIS VWC content products to AMSR-E observations, the technique has the potential for downscaling AMSR-E VWC to higher spatial resolution over moderately cloudy or hazy regions where MODIS reflective bands become contaminated by the atmosphere. During such situations when contaminated MODIS signals cannot be used to obtain the wavelet detail images, MODIS detail images from a preceding time step is used to downscale the current AMSR-E VWC to higher resolutions. This approach of using detail images from the recent past would be justified if the detail images containing the high frequency components of the image change slowly. Correlation analysis of detail images from consecutive time steps shows that this is approximately true, at-least for the low spatial resolution detail images. Our approach yields accuracy of around 77% on the average over the selected study region and temporal period. This technique thus has the potential for ensuring the data continuity of high spatial resolution VWC products, a requirement essential for fire risk monitoring.

Keywords: Fire risk, vegetation water content, wavelet transform.

1. INTRODUCTION

Vegetation water content is one of the critical parameters driving wildland fire susceptibility. The dynamic nature of this parameter ideally requires observations with high temporal and spatial resolutions. The ever increasing expanse of a vulnerable wildland urban interface with substantial human dimensions at stake has reinforced the need for such continuous monitoring. Recently grass fires across a drought-stricken stretch of Oklahoma, Texas and New Mexico burned more than 600,000 acres, destroying at least 470 homes and killing 5 people. Today remote sensing offers the potential of monitoring vegetation water content with the spatial and temporal resolution needed for prevention or better management of wildfires and prescribed fires, the latter becoming increasingly essential for controlling the buildup of fuel and in revitalizing the landscape. Research has shown that remote sensing in the optical, thermal and microwave domain all have the capability of estimating vegetation water content, albeit with uncertainties. The complementary nature of the measurements in the optical and microwave domain implies a need for integrating them for improved coverage in space and time. The potential for synergistic analyses of microwave, infrared and optical data to extract enhanced land surface information has been identified earlier[1-2]. In this study we explore a wavelet based approach for combining vegetation water content observations derived from higher spatial resolution MODIS (500mx500m) and lower spatial resolution AMSR-E (25kmx25km) microwave measurements over sparsely vegetated regions to obtain vegetation water content observations at intermediate resolutions of ~1.5km. The AMSR-E microwave measurements can provide reliable vegetation water content measurements only over sparsely vegetated regions such as grasslands.

They are lower in spatial resolution than optical MODIS measurements but are typically less affected by clouds, water vapor, aerosol or solar illumination, making them complementary to MODIS real time measurements over regions of clouds and haze. The technique presented may be a way for calibrating MODIS VWC to AMSR-E VWC data. Additionally it would be useful for downscaling AMSR-E lower spatial resolution observations to ~1.5 km spatial resolution over cloudy or hazy regions where MODIS optical signals become atmospherically contaminated.

1.1. Vegetation water content using optical remote sensing

Various empirical and physical models utilizing optical measurements have been investigated for estimating vegetation water content. Empirical methods exploiting the obvious correlation between vegetation greenness (chlorophyll content) and moisture content have used indices such as the NDVI or its variations, such as relative greenness, to assess vegetation moisture status[3-5]. Surface temperature (ST) has also been found to improve the sensitivity of optical indices to vegetation moisture, since vegetation temperature increases in drier plants on account of reduced evapotranspiration[6]. Measures such as the ratio of NDVI to ST[7,3] have been found useful. Vegetation indices however are indirect measures of vegetation water and the species dependent nature of relationship between chlorophyll content and moisture content becomes a source of increased uncertainties. More direct methods for vegetation water estimation have typically utilized signals from liquid water absorption channels in the near infrared (NIR) or shortwave infrared (SWIR) and contrasted them with signals from liquid water insensitive channels in the near infrared (NIR). Several indices based on SWIR and NIR reflectances have been proposed such as NDWI, Normalized Difference Water Index [8]; NDII, Normalized Difference Infrared Index [9]; WI, the water index [10], SRWI, the Simple Ratio Water Index[11]; LWCI, the Leaf Water Content Index [12]; GVMI, the Global Vegetation water Moisture Index [13]. Studies [14-15] have shown that SWIR-NIR based indices are related to the weight of water per unit area or the vegetation water content. Relationships between SWIR-NIR based indices and vegetation water content however may be weakened by confounding reflectance contributions from various biophysical (leaf area index, leaf orientation, leaf size), geometric (solar and view zenith and azimuth angles), background (soil and or non-photosynthetically active vegetation) factors. More recently, the inversion of coupled leaf and canopy radiative transfer (RT) models have offered a more physically based approach to vegetation moisture estimation [11,16,17] However RT model inversions are computationally expensive and are prone to ambiguity [18,19] when prior information about various leaf biochemical parameters and leaf and canopy biophysical parameters are unavailable. The unavailability of prior information becomes particularly problematic during rapid real time assessments using RT inversions. The need for lower latency in monitoring the dynamic fire risk environment thus favors the use of fast, site-specific empirical models for assessing local vegetation moisture status albeit with some uncertainties. The simple and computationally fast nature of NIR-SWIR indices make them particularly suitable for real time vegetation moisture and fire risk assessments. In this study we have selected the normalized difference infrared index NDII as a measure of vegetation water content. NDII calculated as $(R_{0.86}-R_{1.64})/(R_{0.86}+R_{1.64})$ is a normalized index using the liquid water absorption 1.64 μm band (MODIS band 6) and the liquid water insensitive 0.86 μm band (MODIS band 2). The two MODIS instruments aboard Terra and Aqua typically makes two daytime observations, one in the morning (10.30am) and the other in the afternoon (1.30pm) respectively. Using MODIS NDII, it is possible to obtain daily vegetation water estimations at spatial resolutions of 500m.

1.2. Vegetation water content using microwave remote sensing

The AMSR-E instrument aboard Aqua measures brightness temperatures at six frequencies (6.92, 10.65, 18.7, 23.8, 36.5, and 89.0 GHz) with vertical and horizontal polarizations at each frequency for a total of 12 channels. It achieves global swath coverage every two days or less, separately for ascending and descending passes, except for a small region near the poles. The mean footprint diameter ranges from 60km at 6.92 GHz to 5km at 89 GHz. The AMSR-E land surface products of surface soil moisture, vegetation water content and surface temperature are available on a daily basis in 25km Equal-Area-Scalable Earth grid (EASE grid) with a global cylindrical, equal area projection true at 30^0N and 30^0S.

The microwave emissivity of snow and water free land surfaces are primarily determined by soil parameters (volumetric moisture content, surface roughness, volume structure and texture) and the overlying vegetation layer characteristics (water content, geometric structure, spatial distributions of stem and leaf components) [20]. An accurate modeling of radiative transfer in the soil vegetation layer requires a large number of parameters, especially if the vertical and horizontal heterogeneity of the vegetation layer is taken into account. However a reduced set of parameters has been shown to be suitable for modeling the soil and vegetation effects since satellite microwave radiometer footprints such as for the AMSR-E are larger than the scales of surface heterogeneity [20]. The AMSR-E land surface parameter algorithm thus uses a simplified physically-based radiative transfer model to retrieve surface soil moisture (g/cm^3), vegetation

water content (kg/m^2) and surface temperature (K) [21]. Sensitivities to parameters (eg. atmospheric water vapor, liquid water, surface roughness, vegetation albedo) are typically an order of magnitude or so less than to these three main variables (surface soil moisture, temperature and vegetation water content) and hence are not dominant factors in the retrieval. The retrieval algorithm uses the two lowest frequencies (6.9 and 10.7 GHz) since modeling surface roughness and vegetation scattering effects above ~10GHz becomes more complex and uncertain. These two frequencies also have better vegetation penetration although at the cost of decreased spatial resolution [21].

Microwave retrievals are more reliable in regions of low vegetation since sensitivities to moisture and vegetation decrease for high vegetation levels, typically above vegetation water content levels of 1.5kg/m [1]. The vegetation water content (VWC) observations which we use in our study can be assumed to be an effective value averaged over the sensor footprint except in situations in which large contrasts occur within the footprint between roughly equal fractions of bare soil and dense vegetation[1]. This area average nature is an important property for combining AMSR-E and MODIS measurements at different spatial resolutions. Based on these observations we have restricted our analysis to primarily homogenous low vegetation grassland regions where microwave measurements are expected to be more reliable.

1.3. Multiresolution analysis using wavelet techniques

Since we have explored the combination AMSR-E vegetation water content observations with MODIS NDII measurements using multi-resolution wavelet analysis, a brief overview of the latter becomes pertinent at this stage. The ensuing description has been adapted from earlier studies[22-25].

The wavelet transform allows multi-resolution decomposition, analysis and reconstruction of remotely sensed images and has potential applications in spatial structure analysis, geometric data merging, data compression, texture analysis and multi-sensor image fusion. The wavelet transform decomposes a function f into a group of functions which are simple dilations and translations of a unique wavelet function Ψ [26]. For a given scale s at a location a, the forward wavelet transform (FWT) of a function f is given by,

$$Wf(s, a)=f * \Psi s\,(a)$$

where, $\Psi s\,(x)=(1/s)\ \Psi(x/s)$ and * denotes the convolution operator. A 2D discrete wavelet transform of an image F_R at resolution R yields four sub-images each at a lower spatial resolution, $2R$: a single context image F_{2R} (approximation coefficients)and three detail images (horizontal coefficients C^H_{2R} , vertical coefficients C^V_{2R} and diagonal coefficients C^D_{2R}). The wavelet decomposition can be interpreted as signal decomposition in a set of independent, spatially-oriented frequency channels. The image F_{2R} corresponds to the lowest frequencies, C^H_{2R} gives the horizontal high frequencies (vertical edges), C^V_{2R} gives the vertical high frequencies (horizontal edges) while C^D_{2R} encompasses the high frequencies in both directions (diagonal). Thus while the approximation image encapsulates a lower resolution version of the original image, the detail images serve to store all local variations at a certain scale in a particular direction.

The forward wavelet transform is achieved by a combination of sub-sampling and convolution with two filters: a low pass filter H and a high pass filter *G*. During sub-sampling every other column or every other row is removed, resulting in reduced spatial dimensions of the four new images. Initially filters H and G are applied on F_R along the columns. The two resulting intermediate images are sub-sampled along the columns before each of them serves as input for the filters H and G applied along the rows. Sub-sampling along the rows ends the process yielding the four final images (Figure.1a).In the process of inverse wavelet transform (IWT), the context and detail images at a particular spatial resolution 2R are used to reconstruct the context image at the next higher resolution level R using inverse filters $\hat{H}$ and $\hat{G}$ (Figure 1b).

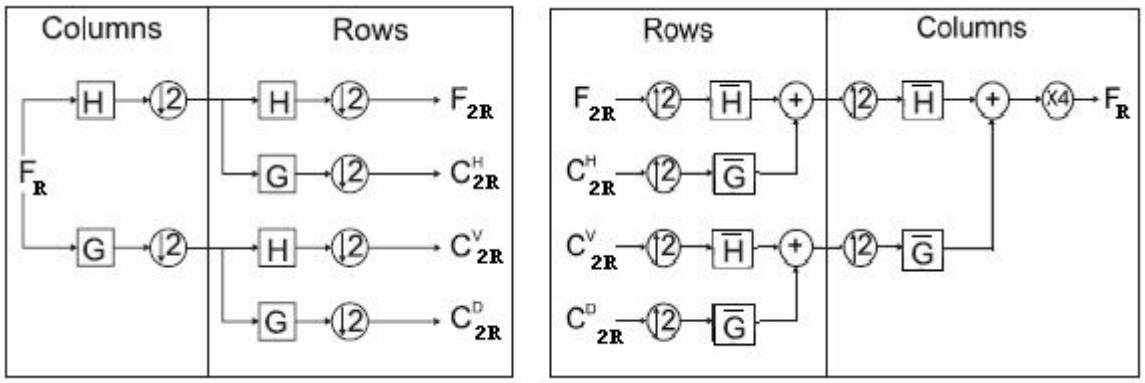

(a) (b)

Figure 1. (from Mertens et al 2004, Ranchin & Wald 2000) (a) Decomposition of F_R (b) Reconstruction of F_R

The context or approximation image obtained in the process of each discrete forward wavelet transform may be successively subjected to additional forward wavelet transforms to generate context and detail images at subsequent lower spatial resolutions, namely 4R, 8R, 16R etc. At every step the spatial resolutions increase by a factor of 2. In the inverse wavelet transform phase, the approximation and detail images at a particular spatial resolution say 16R are used to reconstruct the context image at the next higher spatial resolution 8R. The context image at 8R is then combined with the detail images at 8R to obtain the context image at the next higher spatial resolution 4R. This can be continued until we finally reconstruct the original image at resolution R. Multiesolution wavelet analysis is depicted in Figure 2. Wavelet multiresolution analysis serves to establish the much needed link between different resolution levels of different sensors, and in this case between MODIS and AMSR-E.

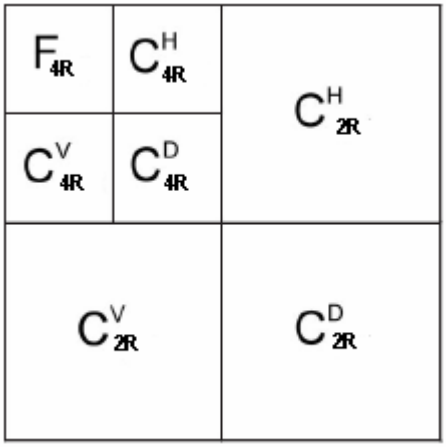

Figure 2. (from Mertens et al 2004, Ranchin & Wald 2000) Multiresolution analysis of source image F_R

Various types of filters are possible during the wavelet decomposition and reconstruction of images. In this study however we have used the simplest filter, namely the Haar filter. The Haar filter has only two coefficients and has the advantage of generating approximation images that are identical to images resulting from an averaging filter. This is an important property which we have exploited in our approach for combining AMSR-E and MODIS observations.

Our basic approach of effecting the combination of high spatial resolution MODIS and low spatial resolution AMSR-E requires two co-registered VWC images one from each sensor. The MODIS image is re-sampled and gridded to a resolution of ~ 0.015^0 and is co-registered with the AMSR-E so that each AMSR-E pixel (25km or ~0.24^0) includes

16x16 pixels of MODIS. In the second step the MODIS image is decomposed successively for four levels using Haar wavelets until we have an approximation image at the spatial resolution of AMSR-E. At this stage the MODIS approximation image is substituted with an appropriately scaled AMSR-E VWC image. The high resolution image at 0.015^0 is reconstructed back by successively applying the inverse Haar transform using the detail images at each stage. The high resolution image thus constructed encapsulates low spatial resolution information from AMSR-E and the detail information from MODIS. This image fusion technique popularly referred to as the substitution method has been used before in many studies to fuse remote sensing images from different sensors. Zhou et al [27] for example used a similar technique to merge Landsat TM and SPOT PAN images by performing an inverse wavelet transform using the approximation image from each TM band and detail images from SPOT PAN. Our technique can be modified over regions of cloud and haze cover where AMSR-E observations are considerably less contaminated than MODIS observations. During such a situation when atmosphere contaminated MODIS images cannot be used to obtain the required detail images, detail images pre-computed from MODIS observations in the recent past may be used to reconstruct the VWC image. The image thus reconstructed should be relatively accurate if the high frequency detail images change very slowly with time. Initial investigation shows that this assumption may be true allowing us the reconstruct high spatial resolution VWC images over cloudy or hazy regions having only AMSR-E data.

2. STUDY AREA AND DATASETS USED

Our study region was selected in a predominantly grassland region of Texas (Figure 3) where microwave observations of VWC are expected to be more reliable due to the low vegetation cover. The region is located between 33.27^0N and 32.11^0N and 100.61W and 98.78W.

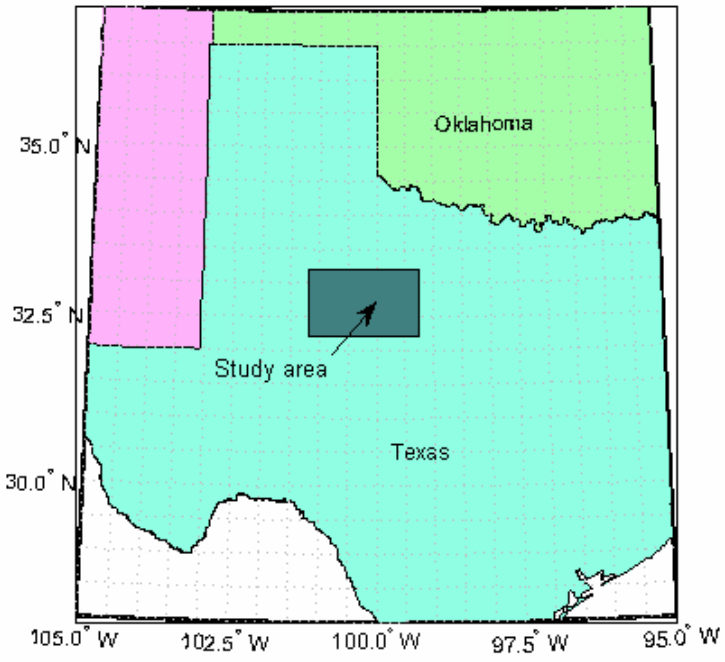

Figure 3. Study Region

We acquired MODIS Terra 8 day surface reflectance products over the study region during the temporal period between August 13th 2005 and December 10th 2005 for a total of 15 eight-day surface reflectance datasets. The MODIS/Terra Surface Reflectance 8-Day L3 Global 500m SIN Grid product, MOD09A1, is a composite of best observations from the previous 8 daily L2G Surface Reflectance products (MYD09GHK). This MODIS product provides estimates of the surface spectral reflectance for each solar reflectance band (bands 1-7) as it would be measured at ground level in the absence of atmospheric scattering or absorption. MODIS band 2 and band 6 surface reflectance were used to obtain the MODIS NDII images. We also acquired AMSR-E/Aqua Daily L3 vegetation water content data

products during the same period. A 5 pixel x 7 pixel AMSR-E VWC image covering the approximately 125kmx175km study region was extracted from each pass (ascending and descending) in each product. The extracted images were averaged over 8 day periods to obtain 5x7 averaged AMSR-E VWC products corresponding to the MODIS 8 day reflectance products. NDII images were re-sampled and re-projected to yield 80x112 pixels (resolution of ~0.015^0) over the same region. The images were co-registered with the AMSR-E images so that each AMSR-E pixel corresponded to a 16x16 sub-block of the MODIS image. Although the proposed technique of combining MODIS and AMSR-E observations is meant to be applicable to daily observations, in this study we have used 8 day products as a first step in investigating and evaluating our approach.

3. METHODOLOGY

Preprocessing of MODIS and AMSR-E data as discussed in the previous section yielded 15 pairs of AMSR-E vegetation water content and MODIS NDII images over the study region. Each AMSR-E pixel corresponded to a 16x16 block of MODIS NDII. In order to derive MODIS VWC images from MODIS NDII, we needed to establish the relationship between NDII and VWC over the region and temporal period selected. As a first step the MODIS NDII was first aggregated to AMSR-E resolution by averaging each 16x16 MODIS NDII pixel block into a single NDII value corresponding to the AMSR-E pixel size. Since the AMSR-E observation has been shown to be area averaged measures over the sensor footprint, AMSR-E VWC and aggregated MODIS NDII (a measure of VWC) is expected to have a linear relationship. This relationship was investigated using linear regression analysis. The linear relationship was reasonably assumed to be applicable at the MODIS resolution and was subsequently used to generate 15 datasets of MODIS VWC.

Each MODIS VWC image was subjected to four levels of wavelet transforms using Haar wavelets, each step yielding detail images at decreasing spatial resolutions (80x112 → 40x56 → 20x28 → 10x14 → 5x7). The final decomposition yielded an approximation context image at the same resolution as AMSR-E. A single level decomposition of an image f yields an approximation image each pixel of which is equal to 2 times the average of a small 2x2 square containing adjacent values from the image f. This is true since we are using the Haar wavelets for our decomposition and it follows that our final approximation image is 2^4 (for 4 levels of decomposition) times the average of a 16x16 sub-block of MODIS VWC. At this stage we have 12 detail images (3 for each of the 4 levels of decomposition) and an approximation image at the same resolution as the AMSR-E VWC. In the final step the approximation image is replaced by AMSR-E VWC image scaled by 16. The reconstruction step then uses the AMSR-E VWC and the pre-computed MODIS detail images to synthesize the higher spatial resolution VWC. This synthesized VWC image is thus a product combined from AMSR-E and MODIS observations.

Our main objective in this study is to investigate whether detail images pre-computed from wavelet decomposition of a MODIS VWC image at a previous time step can be used to reliably reconstruct high spatial resolution VWC at the next time step. Using detail images from a previous time step would become necessary over cloudy or hazy regions where it would not be possible to compute detail images from the contaminated MODIS optical signals. The technique should yield reliable estimations of VWC, if the detail images change slowly over time. Of course the technique would fail if a fire event occurs between the two time steps, since in that case the detail images of the previous step may be drastically different from those at the current time step. In order to investigate the time varying nature of the detail images we analyzed the correlation between pairs of consecutive detail images. In a further step we reconstructed high spatial resolution VWC images using AMSR-E VWC observations from the current time step and MODIS detail images from the previous time step. These proxy high spatial resolution merged VWC images were then compared to the reference high spatial VWC images computed from AMSR-E VWC and MODIS detail images both from the current time-step. The accuracy of the proxy VWC images were evaluated by value-range based classifications of the proxy and actual merged VWC images and determining the extent to which the classifications agree.

4. RESULTS AND DISCUSSION

Our first goal is to investigate the relationship between MODIS NDII and AMSR-E VWC over the region and time selected. This was done by correlating AMSR-E VWC and MODIS NDII aggregated to AMSR-E resolution. Since AMSR-E VWC becomes unreliable at higher values of VWC, we have filtered out (MODIS NDII, AMSR-E VWC) pairs where AMSR-E VWC was greater than $3kg/m^2$. Figure 4 shows the correlation plot. The R^2 value was found to be 0.51 which is reasonably good. Given the multitude of factors (biophysical, geometrical, and atmospheric) that serve to confound the relationship between VWC and sensor observations in the optical and microwave domains, the R^2 value is quite consistent with expected results. The least square linear regression line was found to be VWC=6.68NDII+2.61.

This equation was applied on all the MODIS NDII images to obtain 15 MODIS VWC images over the time period between August and December.

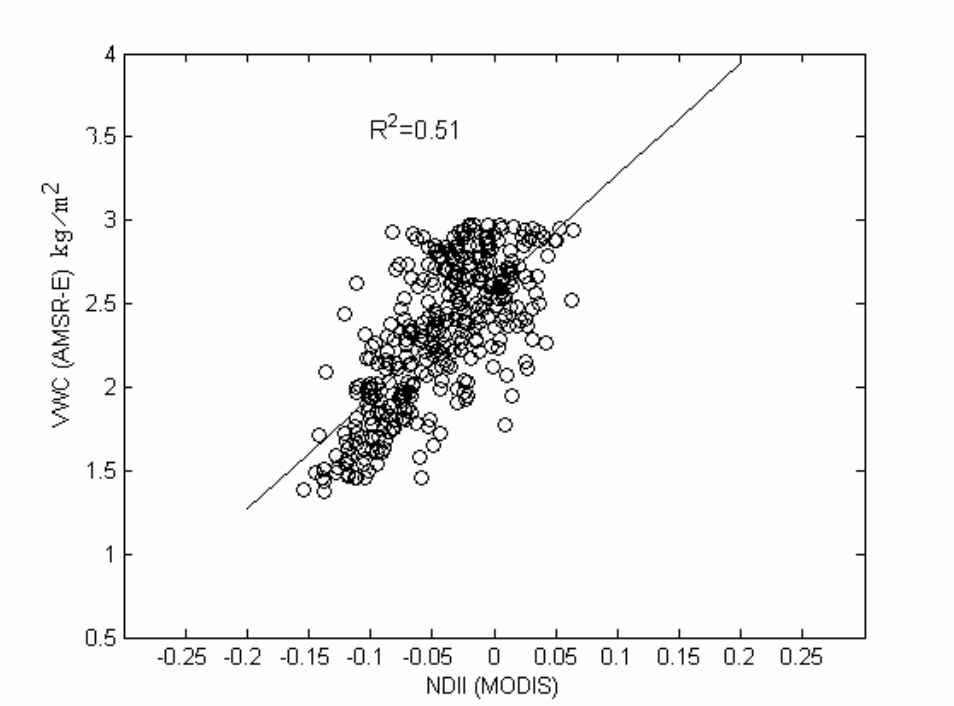

Figure 4. Correlation between AMSR-E VWC (kg/m^2) and aggregated MODIS NDII (p~0)

We applied our merging technique on coincident MODIS VWC and AMSR-E VWC images. The technique as described earlier resorts to successive wavelet decomposition of the high spatial resolution VWC upto 4 levels yielding 3 detail images at each level and an approximation image at the resolution of AMSR-E VWC. At this stage the approximation image is substituted by a scaled AMSR-E VWC and the VWC image is reconstructed to high spatial resolution by inverse wavelet decomposition using the appropriate detail images at each inverse step. Figure 5 shows the results of merging MODIS VWC and AMSR-E VWC for the 8 day period between 25th November and 2nd December 2005. It is evident that AMSR-E VWC acts as a calibrating image. The information from the AMSR-E VWC is downscaled to high resolution pixels while retaining the high frequency components from the MODIS image.

Our primary objective is to investigate whether MODIS detail images from a previous time step could be used along with AMSR-E VWC at the current time step to create the merged VWC product for the current step. This technique, if reasonably accurate would be useful to downscale AMSR-E VWC over cloudy and hazy regions where MODIS reflectances become contaminated rendering them useless in determining the detail images for the current time step. The technique would be reasonably accurate if the MODIS detail images change very slowly with time. In order to investigate this assumption we correlated pairs of detail images at two consecutive time steps. We have 3 detail images at each of the 4 wavelet transform (WT) steps totaling to 12 types of detail images at each time step. We correlated each detail image (horizontal, vertical or diagonal coefficients) at time step t-1 to the corresponding (same WT level) detail image at time t. The mean correlations between consecutive detail image pairs for 12 types of detail images (4 levels x 3 types: horizontal, vertical, diagonal) are given in Table 1. It shows that consecutive detail images at higher levels of decomposition (i..e lower resolution) are more correlated than detail images at lower levels of wavelet decomposition (i.e, higher resolution). This implies details at the highest spatial resolution change more with time than details at a low spatial resolution. The correlations are however reasonably high to investigate the reconstruction of merged VWC products using detail images from a previous time step.

Using inverse wavelet transforms we constructed proxy merged VWC images for a current time step using current AMSR-E VWC and MODIS detail images from the preceding time step. In order to evaluate the accuracy of our

approach we compared the proxy merged VWCs with the actual merged VWC (created using MODIS detail images from the current time step). The comparison was done after value based classification of both the proxy and actual VWC images using value ranges of VWC. The value based classification classified each pixel to one of the 7 classes based on the VWC value at the pixel. The classified proxy merged VWC was compared with the classified actual merged VWC to compute the overall accuracy for each of the 8 day periods except the first one (since the preceding 8 day period wasn't used in our analysis). The average overall accuracy was 77%. Figure 6 shows the actual merged and proxy merged VWC for the 8 day period between 25th November and 2nd December 2005. Figure 7 shows the corresponding classified images.

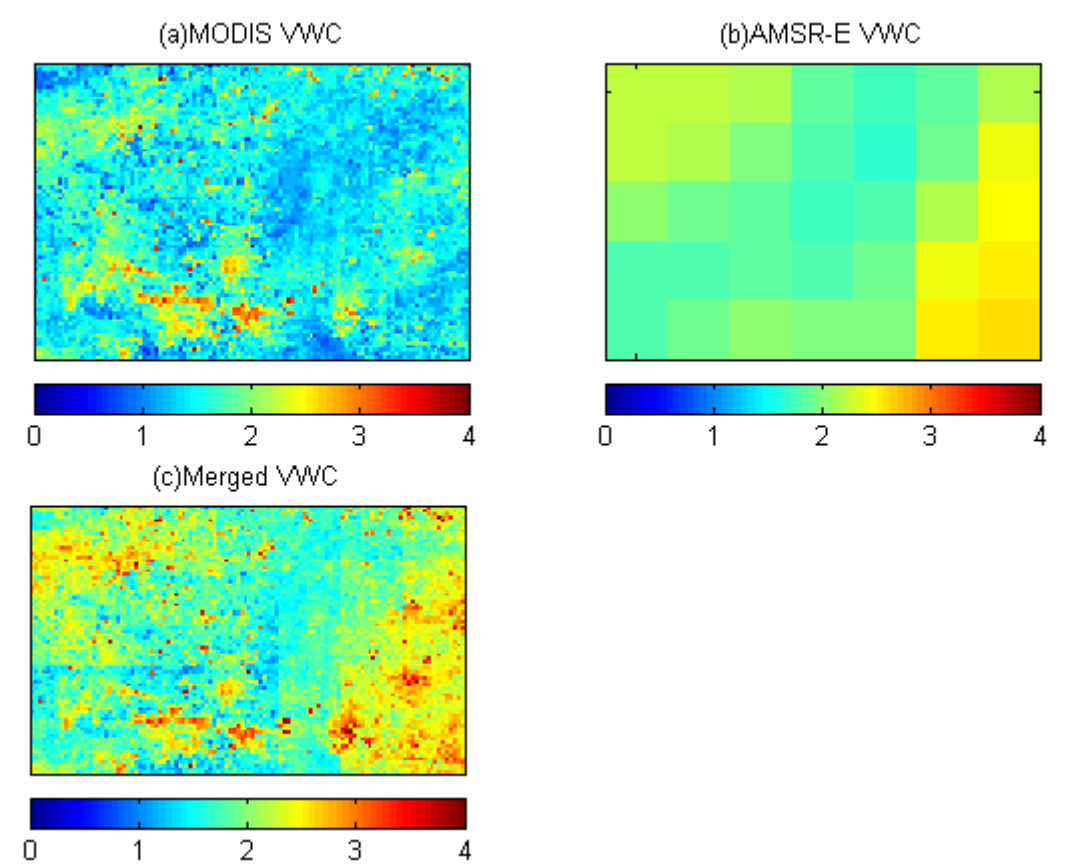

Figure 5. Merging MODIS VWC and AMSR-E VWC using the substitution method for wavelet based image fusion (Period 25th November and 2nd December 2005) (VWC in kg/m^2).

Table 1. Mean correlations between detail images from time step t with detail images from time step t-1

	C^H (horizontal coeffs)	C^D (vertical coeffs)	C^D (diagonal coeffs)
WT level 1	0.76	0.71	0.68
WT level 2	0.86	0.81	0.76
WT level 3	0.91	0.87	0.87
WT level 4	0.94	0.89	0.91

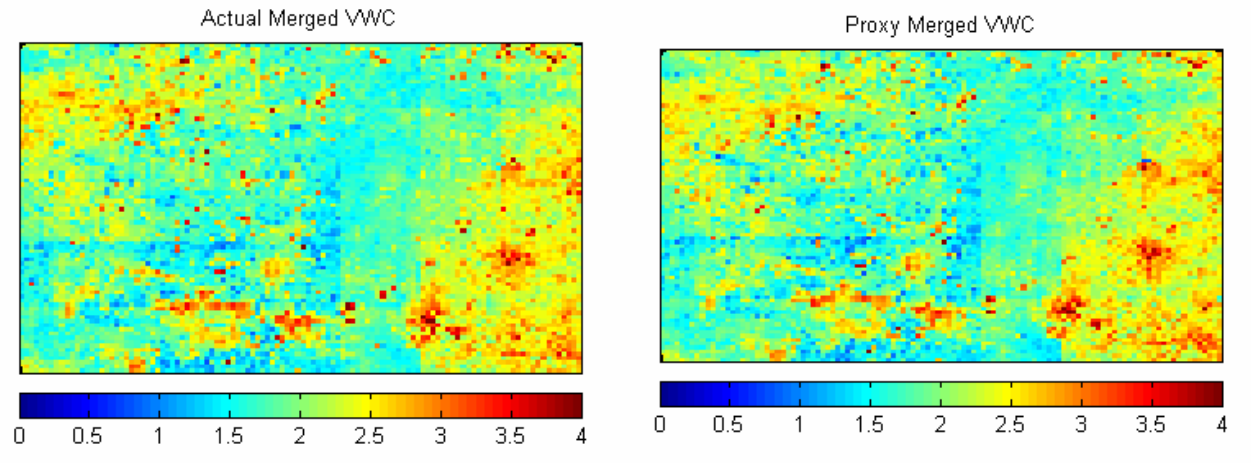

(a) (b)

Figure 6. (a) Actual Merged VWC (kg/m^2) product created using AMSR-E VWC approximation image and MODIS VWC detail images both from the current time step. (b) Proxy merged VWC (kg/m^2) product created using AMSR-E VWC at current step and MODIS VWC detail images from the preceding time step (Current time step: 25th November and 2nd December 2005, Preceding time step: 17th November to 24th November)

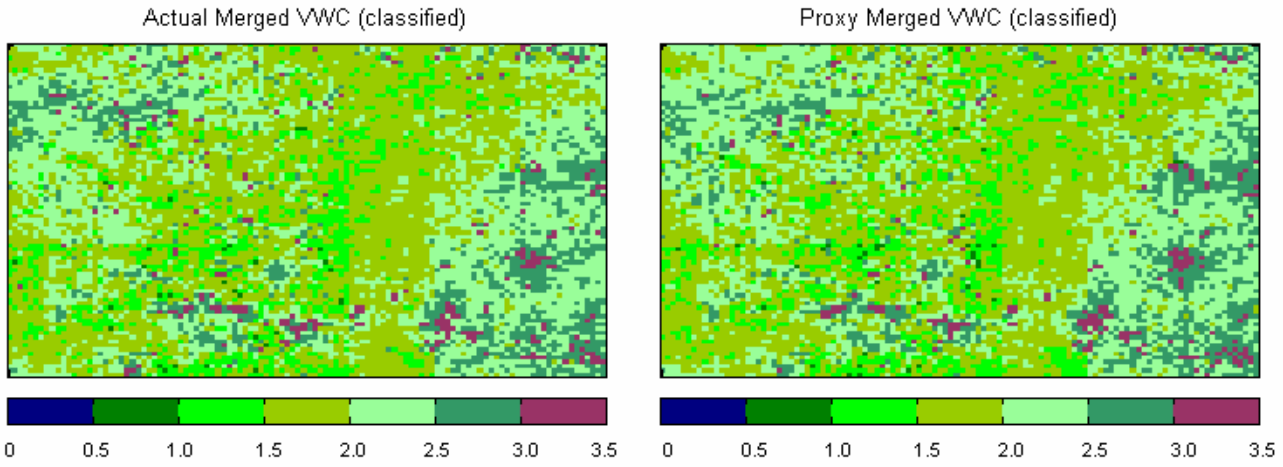

Figure 7. (a) Actual Merged VWC (kg/m^2) product (classified) created using AMSR-E VWC approximation image and MODIS VWC detail images both from the current time step. (b) Proxy merged VWC (kg/m^2) product (classified) created using AMSR-E VWC at current step and MODIS VWC detail images from the preceding time step (Current time step: 25th November and 2nd December 2005, Preceding time step: 17th November to 24th November): Overall accuracy: 75.3%

4. CONCLUSION

We have explored a wavelet decomposition based technique for merging VWC products from optical MODIS and microwave AMSR-E sensors. The technique requires successive decompositions of MODIS VWC products, yielding high frequency detail images at each decomposition step and a single approximation "context" image at a the spatial resolution of AMSR-E VWC product. The approximation image is then substituted by an appropriately scaled AMSR-E

VWC product before reconstructing a merged VWC product. The merged product has information from both MODIS and AMSR-E sensors. The technique is applied over low vegetation regions in Texas grasslands to obtain merged vegetation water content products at intermediate resolutions of ~1.5km. Apart from offering a way to calibrate MODIS VWC content products to AMSR-E observations, the technique has the potential for downscaling AMSR-E VWC to higher spatial resolution over moderately cloudy or hazy regions where MODIS reflective bands become contaminated by the atmosphere. During such situations when contaminated MODIS signals cannot be used to obtain the detail images, MODIS detail images from a preceding time step is used to downscale the current AMSR-E VWC to higher resolutions. This approach of using detail images from the recent past would be justified if the detail images containing the high frequency components of the image change slowly. A correlation analysis of corresponding detail images at consecutive time steps reveal that correlation is reasonably high. Correlation between detail images at higher levels of decomposition (low resolution) are more highly correlated than detail images at lower levels of decomposition (high resolution). This implies that errors would increase as AMSR-E observations are downscaled to higher spatial resolutions. Our approach yields accuracy of around 77% over the selected study region and temporal period. This technique thus has the potential for ensuring the data continuity of high spatial resolution VWC products and could be beneficial for fire risk monitoring.

REFERENCES

1. E.G. Njoku, "Retrieval of land surface parameters using passive microwave measurements at 6-18 GHz," *IEEE Transactions on Geoscience and Remote Sensing,* **37**, pp. 79-93, 1999
2. E.G. Njoku, T.J. Jackson, V. Lakshmi, T.K. Chan, and S.V. Nghiem, "Soil moisture retrieval from AMSR-E," *IEEE Transactions on Geoscience and Remote Sensing,* **41**, pp. 215-229, 2003
3. E. Chuvieco, M. Deshayes, N. Stach, D. Cocero, and D. Riano, "Short-term fire risk: foliage moisture content estimation from satellite data," in *Remote Sensing of Large Wildfires in the European Mediterrranean Basin*, E. Chuvieco, ed.,pp. 17-38, Berlin:Springer-Verlag, 1999
4. E. Chuvieco, D. Riano, I. Aguado, and D. Cocero, "Estimation of fuel moisture content from multitemporal analysis of Landsat Thematic Mapper," *International Journal of Remote Sensing***, 23**, pp. 2145-2162, 2002
5. R.E. Burgan, and R.A. Hartford, "Live vegetation moisture calculated from NDVI and used in fire danger rating," in *Proc. 13th Conference on Fire and Forest Met*. J. Greenlee, ed., Lorne, Australia, Oct. 27-31, 1997.
6. R.D. Jackson, "Remote sensing of biotic and abiotic plant stress," *Annual Review of Phytopathology,* **24,** pp. 265-286, 1986
7. M. Alonso, A. Camarasa, E. Chuvieco, D. Cocero, I. Kyun, M.P. Martin, and F.J. Salas, "Estimating temporal dynamics of fuel moisture content of Mediterranean species from NOAA-AVHRR data," *EARSEL Advances in Remote Sensing* ,**4**, pp. 9-24, 1996
8. Gao, B.C, "NDWI- a normalized difference water index for remote sensing of vegetation liquid water from space," *Remote Sensing of Environment*, **58**, pp. 257-266, 1996
9. M.A. Hardisky, V. Lemas, and R.M. Smart, "The influence of soil salinity, growth form, and leaf moisture on the spectral reflectance of spartina alternifolia canopies," *Photogrammetric Engineering & Remote Sensing*, **49**, pp. 77-83, 1983
10. J. Peñuelas, I. Filella, C. Biel, L. Serrano, and R. Save, "The reflectance at the 950-970 nm region as an indicator of plant water status," *International Journal of Remote Sensing*, **14**, pp. 1887-1905, 1993
11. P.L.J. Zarco-Tejada, C.A. Rueda, and S.L. Ustin, "Water content estimation in vegetation with MODIS reflectance data and model inversion methods," *Remote Sensing of Environment*, **85**, pp. 109-124, 2003
12. E.R. Hunt, B.N. Rock, and P.S. Nobel, "Measurement of leaf relative water content by infrared reflectance," *Remote Sensing of Environment*, **22**, pp. 429-435, 1987
13. P. Ceccato, N. Gobron, S. Flasse, B. Pinty, and S. Tarantola, "Designing a spectral index to estimate vegetation water content from remote sensing data: Part 1. Theoretical approach," *Remote Sensing of Environment*, **82**, pp. 188-197, 2002
14. P. Ceccato, S. Flasse, S. Tarantola, S. Jacquemond, and J.M. Gregoire, "Detecting vegetation water content using reflectance in the optical domain," *Remote Sensing of Environment*, **77**, pp. 22-33, 2001
15. P. Bowyer, and F.M. Danson, "Sensitivity of spectral reflectance to variation in live fuel moisture content at leaf and canopy level," *Remote Sensing of Environment*, **92**, pp. 297-308, 2004
16. S. Jacquemoud, "Inversion of the PROSPECT+SAIL canopy reflectance model from AVIRIS equivalent spectra: theoretical study," *Remote Sensing of Environment*, **44**, pp. 281-292,1993

17. S. Jacquemoud, F. Baret, B. Andrieu, F.M. Danson, and K. Jaggard, K., "Extraction of vegetation biophysical parameters by inversion of the PROSPECT+SAIL models on sugar beet canopy reflectance data. Application to TM and AVIRIS sensors," *Remote Sensing of Environment*, **52**, pp. 163-172, 1995
18. T. Fourty, and F. Baret, "Vegetation water and dry matter contents estimated from top-of-the atmosphere reflectance data: A simulation study," *Remote Sensing of Environment*, **61**, pp. 34-45, 1997
19. B. Combal, F. Baret, M. Weiss, A. Trubuil, D. Mace, A. Pragnere, R. Myneni, Y. Knyazikhin, and L. Wang, "Retrieval of canopy biophysical variables from bidirectional reflectance—using prior information to solve the ill-posed inverse problem," *Remote Sensing of Environment*, **84**, pp. 1–15, 2002
20. E.G. Njoku, and S.K. Chan, "Vegetation and surface roughness effects on AMSR-E land observations," Remote Sensing of Environment, **100**, pp. 190-199, 2006
21. E.G. Njoku, "AMSR land surface parameters, Algorithm theoretical basis document," Jet Propulsion Lab, California Institute of Technology, 1999
22. T. Ranchin, and L. Wald, "Fusion of high spatial and spectral resolution images: The ARSIS concept and its implementation," *Photogrammetric Engineering and Remote Sensing*, **66**, pp. 49– 61, 2000
23. K.C. Mertens, L.P.C. Verbeke, T. Westra, and R. R. De Wulf, "Sub-pixel mapping and sub-pixel sharpening using neural network predicted wavelet coefficients," *Remote Sensing of Environment,* **91**, pp. 34-45, 2004
24. Mohanty, K. K., "The wavelet transform for local image enhancement," *International Journal of Remote Sensing*, **18**, pp. 213–219, 1997
25. C. Yunhao, D. Lei, L. Jing, L. Xiaobing, and S. Peijun, "A new wavelet-based image fusion technique for remotely sensed data," *International Journal of Remote Sensing***, 27**,pp. 1465-1476, 2006
26. C. K. Chui, *An Introduction to Wavelets*, Boston, MA: Kluwer, 1992
27. J. Zhou, D.L. Civco, and J.A. Silander, "A wavelet transform method to merge Landsat TM and SPOT panchromatic data," *International Journal of Remote Sensing,***19**, pp. 743-757, 1998